

# The Cold Gas Content of Bulgeless Dwarf Galaxies

K. Pilkington<sup>1,5</sup>, B.K. Gibson<sup>1,5</sup>, F. Calura<sup>1</sup>, A.M. Brooks<sup>2</sup>, L. Mayer<sup>3,4</sup>, C.B. Brook<sup>1</sup>, G.S. Stinson<sup>1</sup>, R.J. Thacker<sup>5</sup>, C.G. Few<sup>1</sup>, D. Cunnam<sup>6</sup>, and J. Wadsley<sup>7</sup>

<sup>1</sup>*Jeremiah Horrocks Institute, University of Central Lancashire, Preston, PR1 2HE, UK*

<sup>2</sup>*Theoretical Astrophysics, Caltech, 1200 E. California Blvd., Pasadena, CA, 91125, USA*

<sup>3</sup>*Institut für Theoretische Physik, University of Zürich, Zürich, Switzerland*

<sup>4</sup>*Department of Physics, Institut für Astronomie, ETH Zürich, Zürich, Switzerland*

<sup>5</sup>*Department of Astronomy & Physics, Saint Mary's University, Halifax, Nova Scotia, B3H 3C3, Canada*

<sup>6</sup>*Physics Department, University of the Western Cape, Cape Town, South Africa*

<sup>7</sup>*Department of Physics & Astronomy, McMaster University, Hamilton, ON, L8S 4M1, Canada*

Submitted

## ABSTRACT

We present an analysis of the neutral hydrogen (HI) properties of a fully cosmological hydrodynamical dwarf galaxy, run with varying simulation parameters. As reported by Governato et al. (2010), the high resolution, high star formation density threshold version of this galaxy is the first simulation to result in the successful reproduction of a (dwarf) spiral galaxy without any associated stellar bulge. We have set out to compare in detail the HI distribution and kinematics of this simulated bulgeless disk with what is observed in a sample of nearby dwarfs. To do so, we extracted the radial gas density profiles, velocity dispersion (e.g. velocity ellipsoid, turbulence), and the power spectrum of structure within the cold interstellar medium from the simulations. The highest resolution dwarf, when using a high density star formation threshold comparable to densities of giant molecular clouds, possesses bulk characteristics consistent with those observed in nature, though the cold gas is not as radially extended as that observed in nearby dwarfs, resulting in somewhat excessive surface densities. The lines-of-sight velocity dispersion radial profiles have values that are in good agreement with observed dwarf galaxies, but due to the fact that only the streaming velocities of particles are tracked, a correction to include the thermal velocities can lead to profiles that are quite flat. The ISM power spectra of the simulations appear to possess more power on smaller spatial scales than that of the SMC. We conclude that unavoidable limitations remain due to the unresolved physics of star formation and feedback within pc-scale molecular clouds.

**Key words:** galaxies: dwarf – galaxies: evolution – galaxies: formation – methods: N-body simulations

## 1 INTRODUCTION

A traditional problem plaguing the simulation of disk galaxies (e.g. Thacker & Couchman 2001; Sommer-Larsen et al. 2003; Abadi et al. 2003; Governato et al. 2004, 2007; Robertson et al. 2004; Bailin et al. 2005; Okamoto et al. 2005; Sánchez-Blázquez et al. 2009; Stinson et al. 2010, and references therein), within a cosmological context, has been the inability to recover successfully the properties of a truly “late-type” disk and, in particular, those with essentially no associated stellar bulge, similar to classical galaxies such as M33.

Recent work by Governato et al. (2010), though, has produced what appears to be exactly such a bulgeless dwarf, via the imposition of a higher density threshold for star for-

mation ( $100 \text{ cm}^{-3}$ , as opposed to  $0.1 \text{ cm}^{-3}$ , as adopted in the aforementioned earlier generations of simulations), and mass resolution that allows one to identify individual star forming regions.<sup>1</sup> The primary dwarf in their analysis<sup>2</sup> (DG1) forms a shallow central dark matter profile and possesses a pure exponential stellar disk of radial scale  $r_d \sim 1 \text{ kpc}$ , with a stellar bulge-to-disk ratio  $B/D \approx 0.04$  as determined from the  $i$  band light profile.

<sup>1</sup> The higher star formation density threshold can only be applied because the high resolution of the simulation, coupled with heating from the UV background, ensures fragmentation does not occur at unresolved scales.

<sup>2</sup> In addition to the supplementary re-simulation of DG1 described in § 2.

In what follows, we extend this work and examine in detail the cold neutral hydrogen (HI) gas content of the simulated dwarf DG1 along with its low star formation threshold analog, DG1LT, and an updated version of DG1 (called, nDG1) which employs high-temperature metal-line cooling and enhanced supernova energy feedback to compensate for the additional cooling. Our goal is simple: to determine if their HI gas properties agree with recent observational data to an equally successful degree as the stellar component. Studies such as the The HI Nearby Galaxy Survey (THINGS Walter et al. 2008) provide excellent high resolution (spectral and spatial) data against which to compare our simulations. The gas properties of the simulations are compared directly with several of the most recent relevant empirical datasets (Stanimirovic et al. 1999; Tamburro et al. 2009; O’Brien et al. 2010), in order to assess both their strengths and weaknesses.

The cold gas in galaxies is linked directly to underlying star formation processes and associated interstellar medium (ISM) physics; any successful model of galaxy formation should adopt a holistic approach, examining both the gas and star properties in consort. We describe the basic properties of our simulations, before detailing the analyses undertaken; we will present results pertaining to the radial distribution of cold gas within the disks associated with DG1, DG1LT, and nDG1, spatially-resolved velocity dispersion maps of the cold gas, and the spatial distribution of power encoded within the structure of the ISM. We end with a summary of our findings, discussing both the strengths and weaknesses of the current simulations.

## 2 METHOD

### 2.1 Simulations

We have made use of the recent Governato et al. (2010) simulations which produced, for the first time, a late-type dwarf spiral with no associated stellar bulge. A full description of the simulations’ characteristics is provided by Governato et al. (2010), but for context, it is useful to summarise their primary traits.

Using the N-body+SPH (Monaghan 1992) code GASOLINE, a low resolution (25 Mpc box, sufficient to provide realistic torques for these dwarfs), dark matter only simulation was used to identify  $3.5 \times 10^{10} M_{\odot}$  (virial) halos (with typical spin parameters  $\lambda=0.05$ ) for potential (high resolution) re-simulation using a volume renormalisation technique (i.e., “zoom” simulation). New initial conditions were then re-constructed for the primary target halo (called “DG1”), using the relevant low-frequency waves associated with tidal torquing in the low resolution “parent” simulation, but now enhanced with higher spatial frequencies generated after tracing the present-day particles back to the relevant Lagrangian sub-region within the parent. The mass distribution was then sampled at higher resolution in the regions of interest, and more coarsely, further away from the identified halo. Both DG1 and nDG1 have a force resolution of 86pc, while that of DG1LT is somewhat lower (116pc); the initial baryonic (dark) particle mass for DG1 and nDG1 is  $3300 M_{\odot}$  ( $16000 M_{\odot}$ ), while for DG1LT it is  $7800 M_{\odot}$  ( $37000 M_{\odot}$ ). At  $z=0$ , the *i*-band luminosities of

DG1, nDG1, and DG1LT are  $M_i = -16.5$ ,  $-15.8$ , and  $-19.1$ , respectively.

We should re-iterate that each of the three simulations described here (DG1, DG1LT, and nDG1) use the same dark matter halo / assembly history, and differ primarily only in their treatment of the baryonic physics associated with star formation - i.e., either supernova energy feedback efficiency (DG1 vs nDG1) or star formation density threshold resolution (DG1 vs DG1LT). DG1 was simulated using a star formation density threshold of  $100 \text{ cm}^{-3}$ , typical of the densities encountered in giant molecular clouds, rather than the canonical value adopted in earlier simulations ( $0.1 \text{ cm}^{-3}$ ).<sup>3</sup> Other than the increased density threshold, two additional parameterisations were adopted, within the context of the feedback formalism employed: the star formation efficiency ( $\epsilon_{\text{SF}}=0.1$ ) and the fraction of supernova (SN) energy coupled to the ISM ( $\epsilon_{\text{SN}}=0.4$ ). The star formation and feedback are modelled as described in Stinson et al. (2009). Without any additional *ad hoc* adjustments, this high density threshold led to bulgeless dwarf spirals (akin to the classic prototype, M33) with flat (non-centrally concentrated) rotation curves (again, for the first time). Alongside our analysis of the high-threshold DG1 simulation, we provide a parallel analysis of two other simulated dwarfs, DG1LT (the lower-threshold analog, which uses the aforementioned canonical  $0.1 \text{ cm}^{-3}$  threshold, and a star formation efficiency  $\epsilon_{\text{SF}}=0.05$ , with the same initial conditions as that used for DG1), and an updated version of DG1, nDG1 (again with the same initial conditions as DG1 and high density threshold of  $100 \text{ cm}^{-3}$ , but now with high-temperature metal-line cooling, after Shen et al. (2010), and increased thermal energy coupling to the ISM ( $\epsilon_{\text{SN}}=1$ )), in order to better assess the role played by star formation threshold and feedback in “setting” the gas properties of the respective simulations.

To foreshadow the discussion which will follow, perhaps the most problematic aspect of the current analysis is the uncertain numerical “leap-of-faith” that must be made in associating the typically 7000–8000K SPH gas particles, regardless of their local density ( $\sim 0.1\text{--}100 \text{ cm}^{-3}$ ), with star formation (which in nature occurs in clouds and cores with temperatures 2–3 orders-of-magnitude lower than this). Until the effects of cooling by molecular hydrogen are incorporated fully within GASOLINE, this remains an unavoidable limitation of our modeling, but fortunately one whose effects are known and well-understood. We return to this point in § 2.2 and § 3.3.

### 2.2 Analysis

The cold gas properties of DG1, DG1LT, and nDG1 are compared directly with those from comparable dwarfs in The HI Nearby Galaxy Survey (THINGS: Tamburro et al. 2009), in addition to the samples of O’Brien et al. (2010) and Stanimirovic et al. (1999). The bulk properties of DG1 (e.g., mass, luminosity, and gas fraction) are consistent with those observed in nature (e.g. Walter et al. 2008;

<sup>3</sup> GASOLINE employs an ideal gas law equation of state (Wadsley et al. 2004), and the mean molecular weight is implicitly solved for and allowed to vary (Shen et al. 2010).

van den Bosch et al. 2001), and its present-day star formation rate ( $\sim 0.005 M_{\odot}/\text{yr}$ ) and luminosity ( $M_i \approx -16$ ) are (specifically and directly) comparable to those of the three dwarfs from Tamburro et al. (2009), with Holmberg II (HoII) being perhaps the closest direct analog (and, as such, being the empirical counterpart to which we will refer DG1 most often). As noted earlier, the properties which we derive include the radial extent, the velocity dispersion as a function of galacto-centric radius, and the power spectrum of the ISM.

In our work, unless otherwise stated, we label “cold gas” those SPH particles with temperatures less than  $T_{\text{max}}=15000$  K (after Stinson et al. (2006)). The bulk of the gas in DG1 (nDG1) lies near 7000K (9000K), which at face value would appear to be more appropriate for the warm HI phase of the ISM, rather than the cold, star-forming, gas, to which we have associated star formation within the simulation. However, our cooling, despite the inclusion of metal-line cooling, is limited primarily to hydrogen and helium cooling, which can only cool gas down to these temperatures, and as emphasised in Stinson et al (2006; §5.1.1), we are averaging over scales much larger than individual star forming cores. The effect of varying this maximum temperature threshold ( $T_{\text{max}}$ ) for star formation was examined in detail by Stinson et al. (2006), to which the reader is referred. We can summarise that analysis by stating that provided  $T_{\text{max}}$  is chosen to be not too similar in value to that of the mean temperature of the gas particles, its specific value does not critically affect star formation (see also, Shen et al. (2010)). Efforts are underway to implement molecular hydrogen cooling within GASOLINE, after which a quantitative comparison with our results can be undertaken.

DG1LT, the low density threshold analog to DG1, is analysed in parallel, to provide something of a canonical “control” sample. As described in Governato et al. (2010), the properties of DG1LT (e.g., rotation curve, dark matter density profile, bulge-to-disc ratio) are not well-matched to those observed in nature, due to the traditional limitations that the new suite of simulations were designed to overcome in the first place. As a juxtaposition to DG1 though, it is invaluable. The present day star formation rate ( $0.2 M_{\odot}/\text{yr}$ ) and luminosity ( $M_i = -19.1$ ) are much higher than that of DG1 (and the associated stellar mass is correspondingly a factor of ten higher), driven (as described by Governato et al. (2010)) by its adoption of the lower star formation threshold (see Fig 1).

For our analysis, we have generated a new variant of DG1 (labelled nDG1), employing both the same initial conditions and the higher star formation threshold ( $100 \text{ cm}^{-3}$ ). As alluded to earlier, where nDG1 differs from its predecessors is in its inclusion of metal-line cooling (following Shen et al. (2010)) and a more efficient coupling of SN thermal energy to the ISM; qualitatively, we can anticipate this leading to a somewhat more turbulent ISM. On the whole, the star formation rate of nDG1 is suppressed relative to DG1, but extends to lower redshifts (Fig 1, where one can see that the star formation rate from  $8 \lesssim t \lesssim 10$  Gyr is  $\sim 10\times$  higher in nDG1 than in DG1); its luminosity is, not surprisingly, somewhat lower than that of DG1 ( $M_i = -15.8$ , as opposed to  $M_i = -16.5$ ), considering its stellar mass is a factor of two lower ( $M_* \approx 2.1 \times 10^8 M_{\odot}$  vs  $M_* \approx 4.4 \times 10^8 M_{\odot}$ ).

Zeroth (density), first (velocity), and second (velocity

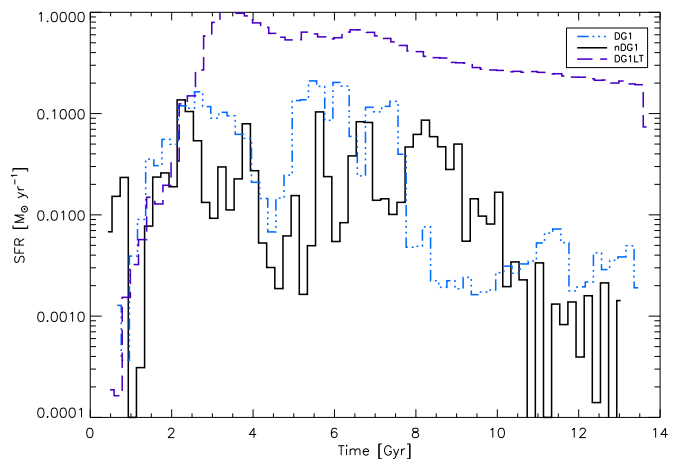


**Figure 1.** The star formation rates of nDG1 (solid line), DG1 (dot-dashed line), and DG1LT (dashed line). Star formation in nDG1 is suppressed overall, relative to DG1, but extends  $\sim 2$  Gyrs beyond the cessation of bulk star formation in DG1 (in the range  $8 \lesssim t \lesssim 10$  Gyrs). There is intermittent star formation in both dwarfs up to the present day, but it has been consistently low for the past  $\sim 3$  Gyrs in nDG1 and  $\sim 5$  Gyrs in DG1. The star formation history of DG1LT is overall considerably higher than its two higher density threshold analogs.

dispersion) moment maps of the simulated neutral hydrogen distributions were generated using TIPSYPY<sup>4</sup>, after matching the  $\sim 40^\circ$  inclination of the dwarfs from the Tamburro et al. (2009) THINGS sample (which, again, includes HoII, our primary analog against which our simulations will be compared, as noted in § 2). The conversion from “cold gas” to “HI” within GASOLINE suffices for the purposes outlined here; the values derived are close to the values one would predict under the assumption of combined photo- and collisional-ionisation equilibrium. All our results were cross-checked using both cold gas and HI moment maps, in addition to further cross-checks undertaken after eliminating high column density HI gas for which the conversion from cold gas to HI is most insecure. The results described here are robust to these choices, and for expediency are not discussed further.

Our velocity dispersion analysis made use of the second HI moment map derived from the line-of-sight dispersion map produced from viewing the DG1, nDG1 and DG1LT simulations with an inclination angle matching that of HoII. For the analysis of the distribution of structural “power” within the cold ISM of the simulations, we again used the zeroth HI moment maps and their Fourier Transforms, and compared the inferred power law spectra with that derived for the SMC by Stanimirovic et al. (1999).

## 3 RESULTS

### 3.1 Radial Density Profiles

We first confirmed independently that the stellar light associated with DG1 was indeed consistent with a pure

<sup>4</sup> [www-hpcc.astro.washington.edu/tools/tipsy/tipsy.html](http://www-hpcc.astro.washington.edu/tools/tipsy/tipsy.html)

exponential of scalelength  $\sim 1$  kpc (i.e. bulgeless) disk (akin to the Type I profiles categorised by, for example, Pohlen & Trujillo (2006)); as shown in the lower panel of Fig 2, this was the case. DG1LT also has a radial (stellar) scalelength of  $\sim 1$  kpc, but shows the classical “problem” of possessing an substantive stellar bulge within the inner kpc ( $B/D \approx 0.2$ ). The stellar disk component of nDG1 is not well-represented by a single pure exponential (cf. DG1); instead, its surface density profile shows a deficit of matter (and light) in the outskirts of the stellar disk (beyond a so-called “break radius” at  $\sim 2-3$  kpc), consistent with the more common Type II profiles observed in nature (e.g. Pohlen & Trujillo 2006; Sánchez-Blázquez et al. 2009); the inner and outer parts of the nDG1 stellar disk show radial scalelengths of  $\sim 2$  kpc and  $\sim 1$  kpc, respectively. The bulge-to-disc ratio of nDG1 matches formally that of DG1, although it is also readily apparent that the surface density (and light) profile of nDG1 shows a high-density stellar “core”, in which  $\sim 10^7 M_{\odot}$  ( $\sim 10\%$  of the nDG1 stellar mass, as a whole) is concentrated within the inner 100 pc. Importantly, this stellar “core” is inconsistent with a bulge. Instead, it consists of a large cluster of stars that was formed in the disk during a merger at high-redshift, and traveled inward with time so that at  $z=0$  it is close to, but not located at, the dynamical center of the galaxy (i.e., it can be seen to rotate about the galaxy center).

The cold gas of DG1 displays a rapid increase in density within  $\sim 1$  kpc. Exterior to this is an extended disk with an exponential scalelength  $r_d \sim 6$  kpc; the cold gas disk truncates at  $\sim 1r_d$ , somewhat short of those observed by Tamburro et al. (2009) and O’Brien et al. (2010), where the respective HI disks are traced out to  $\sim 2-6 r_d$ . Bigiel et al. (2008a) showed that there is an empirical HI upper limit encountered in nature -  $\Sigma_{HI} \gtrsim 9 M_{\odot}/\text{pc}^2$ . This upper limit is represented by the horizontal line in the upper panel of Figure 2. Because we do not yet resolve the microphysics associated with molecular processes on parsec-scales, one might ascribe some fraction of the cold gas in the simulation (particularly that above the upper limit observed by Bigiel et al. (2008a).) to molecular gas. Again using the results from Bigiel et al. for the fraction of  $\text{H}_2/\text{HI}$  as a function of radius (see their Figure 13), we can verify that the high density gas interior to 1 kpc is consistent with being molecular gas. In particular,  $r_{25}$ , the isophotal radius corresponding to 25 mag/arcsec<sup>2</sup>, is 2.0 kpc for DG1. Assuming that as much of the gas can be ascribed to HI as possible (i.e., the upper limit of  $\Sigma_{HI} = 9 M_{\odot}/\text{pc}^2$ ), then the results from Bigiel et al. suggest that  $7.9 M_{\odot}/\text{pc}^2$  would typically be in molecular gas at the innermost radius of DG1, dropping to  $7.2 M_{\odot}/\text{pc}^2$  at 0.8 kpc, and declining rapidly to  $\lesssim 0.1 \text{H}_2/\text{HI}$  at 2 kpc. That is, while the total amount of gas in DG1 is consistent with empirical bulk scaling relations, and the gas within 1 kpc is consistent with being mostly molecular, the cold gas surface densities beyond 1 kpc are too high relative to nature.<sup>5</sup>

It is difficult to interpret the source of this excess gas.

<sup>5</sup> We note that while this is a sample of one, additional simulations from the same suite (e.g., DG2 from (Governato et al. 2010)) show the same behaviour; we have chosen to focus only upon DG1, for clarity.

Perhaps this is gas that should instead be lost from the galaxy in winds? While it may be tempting to suggest that this gas is overly concentrated, comparison of the cold gas scale lengths for these simulated galaxies (which has been fit beyond  $r_{25}$ ) to the scalelengths beyond  $r_{25}$ , in the sample of Bigiel et al. (2010), suggests that the excess gas in these simulations is actually too extended compared to real galaxies. Alternatively, as discussed below for the case of DG1LT, additional star formation in the outskirts of the simulated galaxy disks could decrease the surface density of gas (as it goes instead into stars). While Brooks et al. (2011) showed that the  $B$ -band scale length of DG1 is comparable to observed dwarf galaxies, a factor of 1.5 to 2 increase in size is still allowable to be fully consistent with nature. In fact, preliminary tests of molecular cooling and star formation in GASOLINE suggest that the star formation is more extended at  $z=0$ . Hence, the addition of  $\text{H}_2$  to these simulations may alleviate the problem of this excess gas.

As was the case for the stellar light, the disk of nDG1 is better represented by a “broken”, or two-component exponential, with inner and outer disk scalelengths of  $\sim 2$  kpc and  $\sim 1$  kpc, respectively (with the break occurring near a galactocentric radius of  $\sim 3$  kpc). The arguments of the previous paragraph concerning the excess surface density of cold gas in DG1 applies obviously to nDG1, as well.

Conversely, the cold gas in the disk of DG1LT extends radially to  $\sim 8$  kpc with an essentially flat density profile (formally, with a radial scalelength of  $\sim 18$  kpc - i.e. , the gas disk truncates near  $\sim 0.5r_d$  - again, short of the typical disc in nature, but since the profile is so flat, the formal exponential “scalelength” is somewhat ill-defined). Like DG1, DG1LT also shows a high density cold gas “core” (of mass  $\sim 2 \times 10^6 M_{\odot}$ ), although it is somewhat more extreme, in the sense of it being concentrated solely within the inner  $\sim 100$  pc (note that this is within twice the force softening length). Being more extended, and the gas fraction being an order-of-magnitude lower (Governato et al. (2010); Tbl 2), it is not surprising that the cold gas surface density profile of DG1LT is consistently a factor of  $\sim 3\times$  lower than the empirical upper limit derived by (Bigiel et al. 2008b). However, this result should not be interpreted to mean that DG1LT is the more realistic version of this galaxy simulation. As Governato et al. (2010) and Oh et al. (2011) have demonstrated clearly, the mass of this galaxy is overly concentrated, with a large bulge and peaked inner rotation curve that are inconsistent with observed galaxies in the same mass range.

### 3.2 Velocity Dispersion

We next undertook an examination of the velocity dispersion of the HI disks of DG1, nDG1 and DG1LT, to make a comparison with those observed in various samples of dwarfs in the literature (Crosthwaite et al. 2000, 2001; Tamburro et al. 2009; O’Brien et al. 2010). Observations show that independent of present-day star formation rate, luminosity, or mass, disks possess a characteristic velocity dispersion of  $\sim 8-10$  km/s, rising to  $\sim 12-15$  km/s in the inner star-forming regions (i.e. within  $r_{25}$ , the isophotal ra-

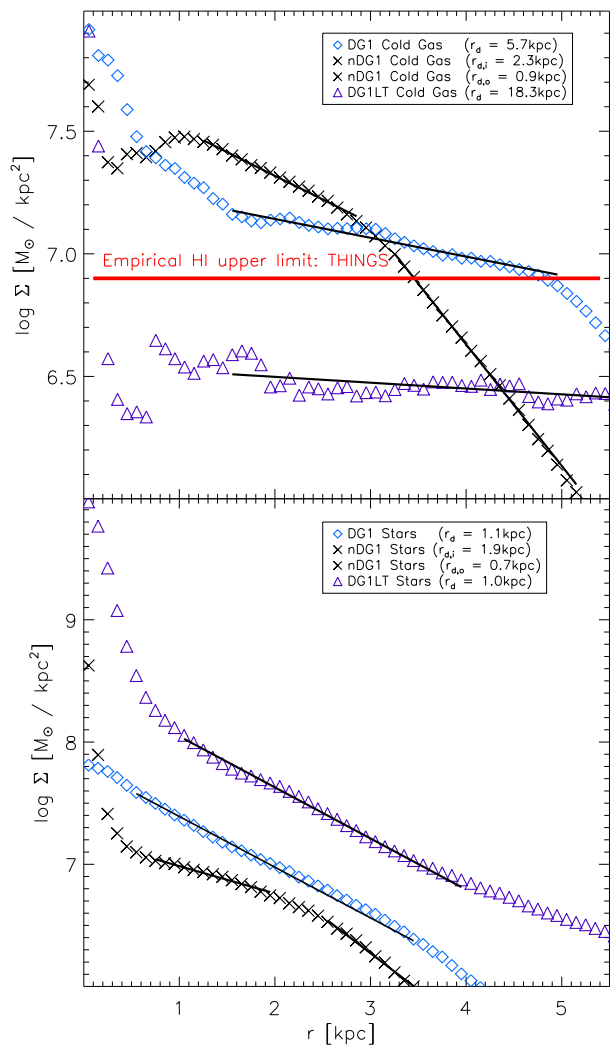


**Figure 2.** Radial gas (top) and stellar (bottom) density profiles for the simulated dwarfs DG1 (diamonds), DG1LT (triangles), and nDG1 (crosses). The thick overplotted lines show the exponential fits to the distributions, from which the noted scalelengths were derived. The stellar component of DG1 obeys a pure exponential of scalelength  $\sim 1$  kpc, with no evidence for a central bulge, while both nDG1 and DG1LT show central cores. Both the stellar and cold gas components of nDG1 are best represented by double exponentials, with a break between the two near  $\sim 3$  kpc. The cold gas of DG1 is distributed in a more extended exponential disk component of scalelength  $\sim 6$  kpc, while that of DG1LT is  $\sim 18$  kpc. The horizontal line in the upper panel corresponds to the empirical upper limit to HI encountered in nature, from the THINGS work (Bigiel et al. 2008a).

dus corresponding to  $25 \text{ mag/arcsec}^2$ .<sup>6</sup> A typical radial velocity dispersion distribution is shown in Fig 3 for HoII (plus signs), from the THINGS sample (Tamburro et al. 2009).

In addition to the curve for HoII, in Figure 3 we also show the corresponding velocity dispersion profiles (line-of-

<sup>6</sup> At the resolutions at which we are working ( $\sim 100$  pc), the velocity dispersions of the molecular and neutral gas are not dramatically different - /citepCros00,Cros01.

sight, assuming again a  $\sim 40^\circ$  inclination, similar to that of HoII) for DG1 (open diamonds), nDG1 (crosses), and DG1LT (triangles), derived from the SPH gas particles’ *streaming velocities* (see below, and van den Bosch et al. (2002)), and for DG1 (filled diamonds), taking into account said particles’ *thermal velocities*. Circular annuli<sup>7</sup> projected on the inclined galaxy were used to set the bins.

For typical Milky Way-scale simulations, the thermal broadening component is often neglected, since the ‘streaming velocity’ of the SPH particle usually dominates over the ‘thermal component’. For our simulated dwarfs, this is clearly inadequate, as the streaming velocity dispersion can be much smaller than the relevant thermal velocity dispersion. To incorporate the latter, we follow the procedure outlined by van den Bosch et al. (2002) (§2.3) and note that the velocity of each particle can be written as  $v = u + w$ , where  $u$  is the mean streaming velocity at the location  $x$  and  $w$  is the particle’s random (thermal) velocity. Because SPH only tracks the streaming motions of the particles, we make use of the internal energy of each particle, in order to derive an appropriate random component to apply to each particle. In practice, we draw random velocities for each Cartesian coordinate from a Gaussian of dispersion  $\sigma = \sqrt{kT/\mu}$  and add those to each of the coordinates of the streaming motion, where  $T$  is the temperature of the gas particle (typically,  $\sim 7000$ – $9000$  K, for our simulations),  $k$  is Boltzmann’s constant, and  $\mu$  is the mean molecular weight of the gas.

Without the inclusion of thermal broadening, both DG1 and nDG1 show extremely (and unphysically) kinematically cold interstellar media compared to DG1LT and, more importantly, dwarfs in nature (compare the crosses and open squares of Figure 3 (simulations) with those of the plus symbols (observations) for a graphic example of the mismatch between unphysical streaming velocity dispersions and those encountered in nature). This is not to imply, however, that DG1LT as presented in Figure 3 is physical. First, and most importantly, as already noted in § 3.1 and, especially, by Governato et al. (2010) and Oh et al. (2011), the rotation curve and dynamics of DG1LT are problematic, as is the associated significant overproduction of the stellar bulge. As can be seen in Fig 1, DG1LT has a star formation rate two orders of magnitude larger than DG1 or nDG1; while this does not impact upon its consistency with the stellar mass-metallicity, luminosity-metallicity, or HI gas fraction-luminosity scaling relations, it does worsen significantly the consistency with the dynamical-to-stellar mass ratio distribution of Blanton et al. (2008). This large star formation rate drives more turbulence, leading to the large streaming velocities for this simulation. We have not included the thermal component for DG1LT in Fig 3, as doing so would only increase its velocity dispersion from  $\sim 12$  km/s to  $\sim 14$  km/s. The inferred line-of-sight velocity dispersion profile for DG1, after application of the above thermal broadening (which effectively amounts to a  $\sigma \sim 7$ – $9$  km/s broadening of the essen-

<sup>7</sup> Technically, elliptical annuli should be used, but our results are not sensitive to this choice, at these inclination angles; in addition, we re-measured the velocity dispersion profile on the raw THINGS data for HoII using circular annuli, to ensure self-consistency with our analysis of the simulations.

tially negligible  $\sim 1$  km/s streaming motions), is represented by the filled squares in Figure 3.

The characteristic velocity dispersions of the cold gas within DG1 and nDG1 are comparable to those encountered in nature ( $\sim 8$ – $10$  km/s - Tamburro et al. (2009)) when thermal velocities are considered. The thermally broadened velocity dispersion profile of DG1 shows a few enhanced features (near  $0.5r_{25}$ ). These are due to high temperature gas particles in and around superbubbles blown by SNe feedback (discussed further below and shown in Figure 4). By design, including a random thermal component to the velocity dispersion accentuates these features. However, by chance, the particular timestep we examine here for nDG1 does not show any bubbles (though does at previous timesteps), and hence no thermal features are introduced into the profile of this simulation. As can be seen from the streaming-only profiles for these galaxies, both have slightly higher macroscopic velocity dispersions in the inner few hundred parsecs. However, in DG1 this gas is  $\sim 35\%$  hotter than the rest of the disk, while in nDG1 it is cooler by a similar factor. Figure 3 shows that, when this is considered in the thermally broadened velocity dispersions, it has the effect of maintaining the higher velocity dispersion structure in the inner region of DG1, while “washing out” the inner structure in nDG1. This result highlights a conundrum in terms of comparing the velocity dispersion profiles of these dwarf galaxy simulations to real dwarfs.

A more subtle effect of imposing the random thermal velocity perturbation to each particle’s streaming motion is that the velocity ellipsoid of the cold gas becomes necessarily isotropic, disguising any anisotropies that might have been present in the streaming motions (i.e., young stars, and the cold gas from which they formed, will necessarily have different velocity ellipsoids). For example, for DG1 (nDG1), the radial, azimuthal, and vertical velocity dispersions inferred from the cold gas particles’ streaming motions, measured at  $\sim 0.5r_d$ , are  $\sigma_r \approx 4$  km/s ( $\sim 6$  km/s),  $\sigma_\phi \approx 3$  km/s ( $\sim 6$  km/s), and  $\sigma_z \approx 1$  km/s ( $\sim 2$  km/s) – i.e.,  $\sigma_r:\sigma_\phi:\sigma_z \approx 3:3:1$  (anisotropic). After thermal broadening, the derived respective velocity dispersions are  $\sigma_r \approx 8.5$  km/s ( $\sim 10$  km/s),  $\sigma_\phi \approx 8$  km/s ( $\sim 10$  km/s), and  $\sigma_z \approx 7.5$  km/s ( $\sim 8.5$  km/s) – i.e.,  $\sigma_r:\sigma_\phi:\sigma_z \approx 1:1:1$  (isotropic). What this means is that an unavoidable outcome of our current inability to resolve pc-scale molecular heating and cooling processes within the simulations is the lack of any significant correlation between velocity dispersion and galactocentric radius and/or underlying star formation. Until we can resolve densities (and temperatures) corresponding to the cores of molecular clouds, this apparent mismatch between observations and simulations would appear difficult to avoid.<sup>8</sup>

<sup>8</sup> It might be tempting to conclude that since the enhanced feedback did not result in a *significantly* higher line-of-sight velocity dispersion, this is consistent with the earlier work of Dib et al. (2006) and Petric & Rupen (2007), who concluded that supernova feedback alone was insufficient to provide turbulent heating to the cold ISM in excess of a few km/s; in light of the fact that we are not resolving the ISM heating and cooling processes at pc and sub-pc scales, we feel it premature to draw such a conclusion from this aspect of our analysis.

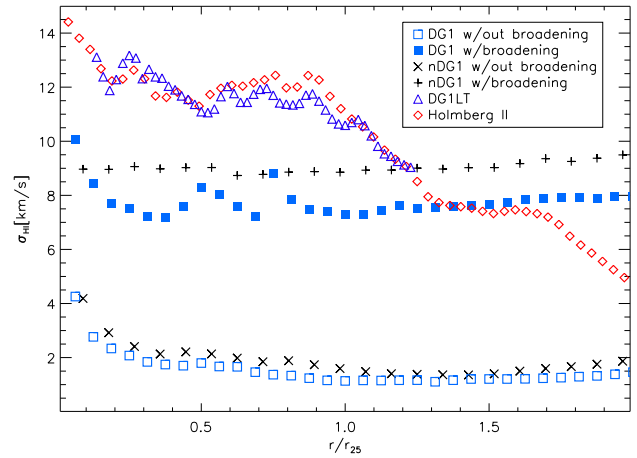


**Figure 3.** Radial behaviour (in units of the B-band  $r_{25}$  - i.e. the isophotal radius corresponding to 25 mag/arcsec<sup>2</sup> or, roughly, to the extent of the star forming disk) of the HI line-of-sight velocity dispersion of the DG1 (open squares), DG1LT (open triangles), and nDG1 (crosses) simulations, derived from the SPH gas particles’ ‘streaming velocities’ (after van den Bosch et al. (2002)), in addition to the true HI line-of-sight velocity dispersion profile for DG1 (filled squares) and nDG1 (plus signs), after correcting the streaming velocities isotropically for their internal thermal energies. Also shown is a representative dwarf spiral from the THINGS (Tamburro et al. 2009) sample (HoII: open diamonds). note:  $r_{25}$  is 2.0 kpc, 5.5 kpc, 1.4 kpc, and 3.3 kpc, respectively, for DG1, DG1LT, nDG1, and HoII.

### 3.3 Power Spectrum and Superbubbles

Following Stanimirovic et al. (1999), we generated the Fourier Transform of the HI moment zero maps of DG1, nDG1, and DG1LT – each shown in Figure 4 at the same spatial scale ( $14 \times 14$  kpc) with the same limiting HI column density ( $N(\text{HI}) > 1 \times 10^{19} \text{ cm}^{-2}$ ) – after first convolving the maps with a 100 pc Gaussian, to mimic the typical beam-smearing present within THINGS data for HoII (Tamburro et al. 2009). Circular annuli in Fourier space were then employed to derive the average power in the structure of the ISM on different spatial scales. Figure 5 shows the derived power spectra for the simulations DG1, nDG1, and DG1LT, and that for the Small Magellanic Cloud (SMC), re-derived for self-consistency, using the HI datacube of Stanimirovic et al. (1999). Grossly speaking, the distributions can be represented by a power law of the form  $P \propto k^\gamma$ , with  $\gamma = -3.5$  for DG1,  $\gamma = -3.4$  for DG1LT, and  $\gamma = -4.2$  for nDG1, and  $\gamma = -3.2$  for the SMC (consistent with that found originally by Stanimirovic et al. (1999), and consistent with the power spectrum expected when HI density fluctuations dominate the ISM structure, rather than turbulent velocity fluctuations, which dominate the spectrum when isolating ‘thin’ velocity slices).

There are several points to highlight from Fig 5: (i) the SMC shows no evidence for departure from a pure power law, and hence there does not appear to be any obvious preferred HI cloud size in nature; (ii) broadly speaking, both DG1 and DG1LT are shallower than nDG1 (i.e., possess more power on smaller scales, rather than larger, relatively speaking); put another way, the enhanced feedback associ-

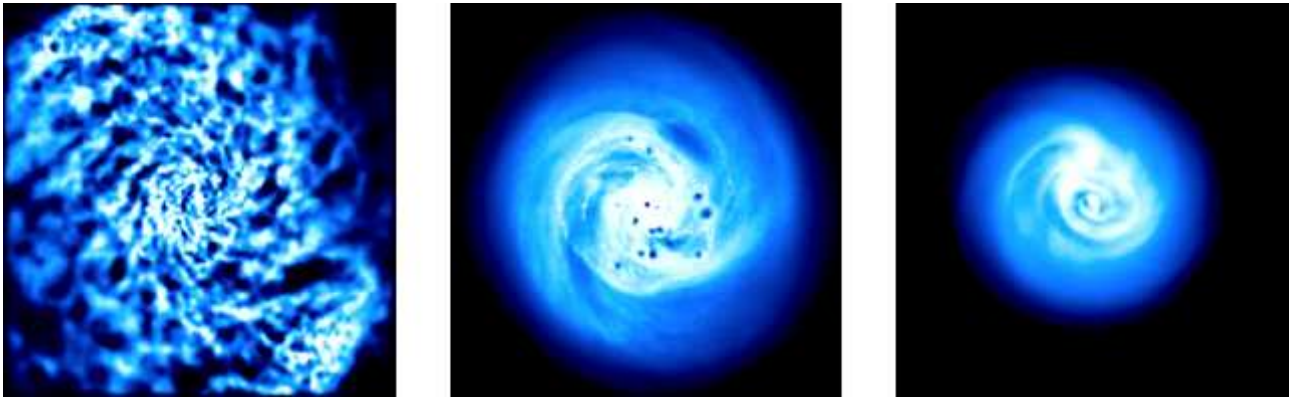


**Figure 4.** Neutral hydrogen (HI) moment zero maps of the three simulations analysed here - from left to right: DG1LT, DG1, and nDG1. Each panel has dimensions  $14 \times 14$  kpc; a lower column density threshold of  $N(\text{HI}) = 1 \times 10^{19} \text{ cm}^{-2}$  was employed for each map.

ated with nDG1 shifts power in the simulated ISM from smaller scales to larger scales, just as one might expect; (iii) each of the simulations shows a greater departure from a pure power law, than does the SMC; the most obvious departure from a power law is perhaps seen in the enhanced power on  $\sim 400$ – $500$  pc scales in nDG1. This enhanced power corresponds to the “radial cadence”, or frequency, of the tightly-wound spiral structure in the inner few kpcs of the simulation (apparent in the right-most panel of Figure 4).

Finally, from the present-day moment zero column density map of DG1 (middle panel of Figure 4), we identified 13 SNe-driven superbubbles in its cold ISM. While we do not wish to belabour the point when employing such small-number statistics, it is re-assuring to note that upon plotting the superbubble size distribution, the data were consistent with a power law slope between  $-1.5$  and  $-2.0$  (dependent upon normalisation). Such slopes are entirely consistent with those observed in nearby dwarfs (Oey & Clarke 1997).

#### 4 DISCUSSION

One immediate concern arising from our analysis relates to the issue of extracting “neutral hydrogen” from the simulations’ “cold gas” (which in some sense consists of both molecular and neutral hydrogen). Because the high-density regions within the simulation have densities more akin to molecular, rather than neutral, clouds, it is important to explore the definition of “neutral” employed here.<sup>9</sup> To do this, we re-generated HI moment maps, but now restricting the gas included to only those particles with densities near the classical value of  $\sim 0.1 \text{ cm}^{-3}$ . As expected, this eliminated the unrealistically high neutral hydrogen column densities in the highest density regions, but at the expense of leading to vertical density profiles that bore little resemblance to the Gaussian profiles observed in nature (O’Brien et al. 2010). Such an extreme “cut” to the definition of neutral hydrogen also led to a radial profile that

<sup>9</sup> In large part, this was motivated by the fact that in “column density space”, these high-density regions possess column densities close to  $10^{22} \text{ cm}^{-2}$ , higher than those observed in nature; this is a limitation of the conversion employed within GASOLINE.

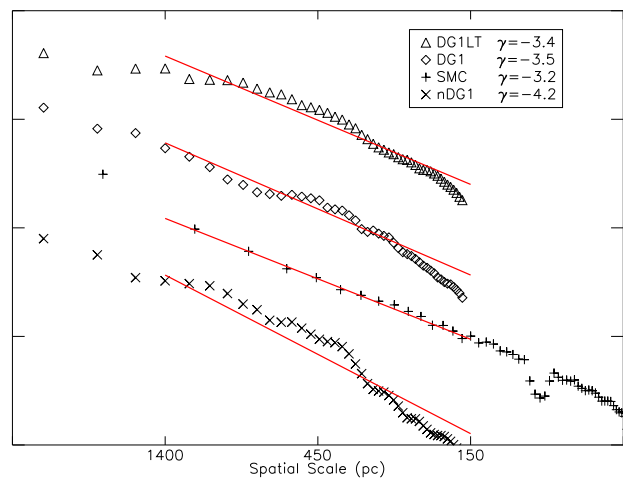


**Figure 5.** Spatial power spectra of the cold ISM of DG1 (diamonds), DG1LT (triangles), nDG1 (crosses), and the SMC (plus signs). Power law slopes of  $-3.5$ ,  $-3.4$ ,  $-4.2$  and  $-3.2$  are over-plotted for DG1, DG1LT, nDG1, and the SMC, respectively. The “break” in the SMC power spectrum is due to a missing baseline in the Stanimirovic et al. (1999) ATCA dataset. The power spectra for the three simulations have been truncated at  $\sim 2$  resolution elements ( $2 \times \text{FWHM}$  of the adopted Gaussian beam:  $\sim 200$  pc).

bore little resemblance to an exponential. We found no density cut which impacted favourably on the observable properties of DG1. For these simulations, because density and temperature are closely correlated in the relevant regime ( $T \lesssim 30000 \text{ K}$ ;  $\rho \gtrsim 0.001 \text{ cm}^{-3}$ ), the above analysis is degenerate to cuts in volume density or temperature.

It is important to note that the primary process responsible for driving bulk properties in the simulation is the star formation and feedback prescription. Governato et al. (2010) demonstrated that star formation had a larger effect on the rotation curve of our simulated galaxy than resolution (see their Figure 5). The gas properties presented in this paper are primarily the result of the star formation prescription, and thus it is imperative to use a star formation and feedback prescription that is physically motivated. Until metal-dependent  $\text{H}_2$  creation and cooling is added to the

simulations, it is not clear how much HI, as opposed to H<sub>2</sub>, should be present in the simulation, how it might be distributed as a function of radius, and what impact it will have on the resulting disk.

After applying the physically-motivated  $\sim 8$  km/s thermal broadening to the Cartesian coordinates of the SPH particles' streaming motion, the inferred *characteristic* velocity dispersions for the cold gas were a reasonable match to those observed in nature (albeit, at the unavoidable expense of recovering any correlation between velocity dispersion and galactocentric radius and/or global star formation in the disk, in addition to the imposition of an isotropic velocity ellipsoid to the cold gas, and the young stars which form from this gas). Beyond the aforementioned issue of the lack of a self-consistent treatment of molecular cooling processings on sub-parsec scales, one must also be aware that at the resolutions of these simulations, we are still missing unresolved star forming regions and associated turbulence. The nature of these missing sources is an active area of debate, but magnetorotational instability (MRI) is one of the favoured mechanisms capable of providing a non-negligible amount of turbulence (e.g. Wang & Abel 2009; Piontek & Ostriker 2007; Mac Low 2009)

Enhancing the supernovae energy feedback, as was done for simulation nDG1, at these resolutions, had a marginal impact on the SPH particles' streaming velocities (at the  $\sim 20\%$  level), which in turn meant that its impact on the velocity dispersion profiles was also minimal. This is not surprising, as the increased energy deposition was used in order to offset the effect of the newly included high-temperature metal-line cooling. Without the inclusion of extra SN energy, the additional cooling that comes from metal lines leads to more star formation than in the case of DG1. As shown by Oh et al. (2011), the stellar mass of DG1 is in good agreement with galaxies at similar halo masses, as observed by THINGS. If high-temperature metal-line cooling had been added with  $\epsilon$ SN held constant, nDG1 would have overproduced stars for galaxies in a comparable halo mass range. However, the enhanced feedback seems to have steepened the spatial power spectrum of the cold ISM of nDG1 relative to DG1, making it less consistent with the power spectrum observed for the SMC. It is unclear, however, how the power spectrum varies with the instantaneous SFR and if this result holds across time.

Capturing all the relevant ISM physics necessary to recover the full spectrum of turbulence sources at pc and sub-pc scales remains an outstanding challenge. Despite these limitations, the simulated dwarf galaxies presented here have been shown to possess bulk characteristics consistent with those observed in nature, including adherence to scaling relations such as the size-luminosity, size-velocity, and luminosity-velocity (Brooks et al. 2011). Additionally, the star formation and feedback prescription used in these simulations has been shown to result in a realistic mass-metallicity relationship as a function of time, and consume gas at a rate that reproduces the incidence rate and metallicities of both QSO-Damped Lyman Alpha (DLA) and GRB-DLA systems (Brooks et al. 2007; Pontzen et al. 2008; Pontzen & Pettini 2009).

Hence, it is clear that our simulations remain extremely successful in recovering many of the *global* optical and dynamical properties of realistic bulgeless dwarfs.

That is, although the microphysics of the ISM cannot be fully captured at the force resolutions that must be used currently in cosmological simulations, this does not largely impact the bulk macrophysics such as the rotation curves (stellar and dark matter mass profiles), angular momentum content, etc. On the other hand, we have seen that higher resolutions and adoption of more realistic physics for star formation leads to simulated galaxies that better reproduce the properties of observed galaxies (e.g., Booth et al. 2007; Robertson & Kravtsov 2008; Tasker & Bryan 2008; Saitoh et al. 2008; Ceverino & Klypin 2009; Governato et al. 2010). The work presented here highlights paths for future improvement in the implementation of ISM physics in cosmological simulations, and provides useful tests for reassessment once metal-dependent H<sub>2</sub> cooling and star formation has been added to GASOLINE and other cosmological simulation codes.

## ACKNOWLEDGMENTS

We wish to thank the THINGS team for their insights and access to their exceptional dataset, in addition to a number of helpful discussions with F. Governato and A. Pontzen and comments from the referee which led to a vastly improved manuscript. BKG and CBB acknowledge the support of the UK's Science & Technology Facilities Council (ST/F002432/1). KP acknowledges the support of STFC through its PhD Studentship programme (ST/F007701/1). RJT acknowledges support from NSERC, CFI, the CRC program, and NSRIT. KP and BKG acknowledge visitor support from Saint Mary's University. We thank the DEISA consortium, co-funded through EU FP6 project RI-031513 and the FP7 project RI-222919, for support within the DEISA Extreme Computing Initiative, and the UK's National Cosmology Supercomputer (COSMOS), NASA's Advanced Supercomputing Division, TeraGrid, the Arctic Region Supercomputing Center, and the University of Central Lancashire's High Performance Computing Facility.

## REFERENCES

- Abadi M. G., Navarro J. F., Steinmetz M., Eke V. R., 2003, *ApJ*, 591, 499
- Bailin J., Kawata D., Gibson B. K., Steinmetz M., Navarro J. F., Brook C. B., Gill S. P. D., Ibata R. A., Knebe A., Lewis G. F., Okamoto T., 2005, *ApJ*, 627, L17
- Bigiel F., Leroy A., Walter F., Blitz L., Brinks E., de Blok W. J. G., Madore B., 2010, *ArXiv e-prints*
- Bigiel F., Leroy A., Walter F., Brinks E., de Blok W. J. G., Madore B., Thornley M. D., 2008a, *AJ*, 136, 2846
- Bigiel F., Leroy A., Walter F., Brinks E., de Blok W. J. G., Madore B., Thornley M. D., 2008b, *AJ*, 136, 2846
- Blanton M. R., Geha M., West A. A., 2008, *ApJ*, 682, 861
- Booth C. M., Theuns T., Okamoto T., 2007, *MNRAS*, 376, 1588
- Brooks A. M., Governato F., Booth C. M., Willman B., Gardner J. P., Wadsley J., Stinson G., Quinn T., 2007, *ApJ*, 655, L17



- Brooks A. M., Solomon A. R., Governato F., McCleary J., MacArthur L. A., Brook C. B. A., Jonsson P., Quinn T. R., Wadsley J., 2011, *ApJ*, 728, 51
- Ceverino D., Klypin A., 2009, *ApJ*, 695, 292
- Crosthwaite L. P., Turner J. L., Ho P. T. P., 2000, *AJ*, 119, 1720
- Crosthwaite L. P., Turner J. L., Hurt R. L., Levine D. A., Martin R. N., Ho P. T. P., 2001, *AJ*, 122, 797
- Dib S., Bell E., Burkert A., 2006, *ApJ*, 638, 797
- Governato F., Brook C., Mayer L., Brooks A., Rhee G., Wadsley J., Jonsson P., Willman B., Stinson G., Quinn T., Madau P., 2010, *Nature*, 463, 203
- Governato F., Mayer L., Wadsley J., Gardner J. P., Willman B., Hayashi E., Quinn T., Stadel J., Lake G., 2004, *ApJ*, 607, 688
- Governato F., Willman B., Mayer L., Brooks A., Stinson G., Valenzuela O., Wadsley J., Quinn T., 2007, *MNRAS*, 374, 1479
- Mac Low M., 2009, in *Revista Mexicana de Astronomia y Astrofisica Conference Series Vol. 36 of Revista Mexicana de Astronomia y Astrofisica*, vol. 27, *Magnetic Effects in Global Star Formation*. pp 121–127
- Monaghan J. J., 1992, *ARA&A*, 30, 543
- O’Brien J. C., Freeman K. C., van der Kruit P. C., 2010, *A&A*, 515, A62+
- Oey M. S., Clarke C. J., 1997, *MNRAS*, 289, 570
- Oh S., Brook C., Governato F., Brinks E., Mayer L., de Blok W. J. G., Brooks A., Walter F., 2011, *ArXiv e-prints*
- Okamoto T., Eke V. R., Frenk C. S., Jenkins A., 2005, *MNRAS*, 363, 1299
- Petric A. O., Rupen M. P., 2007, *AJ*, 134, 1952
- Piontek R. A., Ostriker E. C., 2007, *ApJ*, 663, 183
- Pohlen M., Trujillo I., 2006, *A&A*, 454, 759
- Pontzen A., Governato F., Pettini M., Booth C. M., Stinson G., Wadsley J., Brooks A., Quinn T., Haehnelt M., 2008, *MNRAS*, 390, 1349
- Pontzen A., Pettini M., 2009, *MNRAS*, 393, 557
- Robertson B., Yoshida N., Springel V., Hernquist L., 2004, *ApJ*, 606, 32
- Robertson B. E., Kravtsov A. V., 2008, *ApJ*, 680, 1083
- Saitoh T. R., Daisaka H., Kokubo E., Makino J., Okamoto T., Tomisaka K., Wada K., Yoshida N., 2008, *PASJ*, 60, 667
- Sánchez-Blázquez P., Courty S., Gibson B. K., Brook C. B., 2009, *MNRAS*, 398, 591
- Shen S., Wadsley J., Stinson G., 2010, *MNRAS*, 407, 1581
- Sommer-Larsen J., Toft S., Rasmussen J., Pedersen K., Götz M., Portinari L., 2003, *Ap&SS*, 284, 693
- Stanimirovic S., Staveley-Smith L., Dickey J. M., Sault R. J., Snowden S. L., 1999, *MNRAS*, 302, 417
- Stinson G., Seth A., Katz N., Wadsley J., Governato F., Quinn T., 2006, *MNRAS*, 373, 1074
- Stinson G. S., Bailin J., Couchman H., Wadsley J., Shen S., Nickerson S., Brook C., Quinn T., 2010, *MNRAS*, 408, 812
- Stinson G. S., Dalcanton J. J., Quinn T., Gogarten S. M., Kaufmann T., Wadsley J., 2009, *MNRAS*, 395, 1455
- Tamburro D., Rix H., Leroy A. K., Mac Low M., Walter F., Kennicutt R. C., Brinks E., de Blok W. J. G., 2009, *AJ*, 137, 4424
- Tasker E. J., Bryan G. L., 2008, *ApJ*, 673, 810
- Thacker R. J., Couchman H. M. P., 2001, *ApJ*, 555, L17
- van den Bosch F. C., Abel T., Croft R. A. C., Hernquist L., White S. D. M., 2002, *ApJ*, 576, 21
- van den Bosch F. C., Burkert A., Swaters R. A., 2001, *MNRAS*, 326, 1205
- Wadsley J. W., Stadel J., Quinn T., 2004, *New Astronomy*, 9, 137
- Walter F., Brinks E., de Blok W. J. G., Bigiel F., Kennicutt R. C., Thornley M. D., Leroy A., 2008, *AJ*, 136, 2563
- Wang P., Abel T., 2009, *ApJ*, 696, 96